PHYSICAL REVIEW C VOLUME 48, NUMBER 5 NOVEMBER 1993

Relativistic microscopic description of proton-nucleus scattering at intermediate energies

G. Q. Li and R. Machleidt
Department of Physics, University of Idaho, Moscow, Idaho 83843

R. Fritz and H. Müther
Institut für Theoretische Physik, Universität Tübingen, 72076 Tübingen, Germany

Y. Z. Zhuo
Institute of Atomic Energy, P. O. Box 275, Beijing 102413, China
and Institute of Theoretical Physics, P. O. Box 2735, Beijing 100080, China
(Received 9 July 1993)

We study elastic proton-nucleus scattering at intermediate energies. The nucleon-nucleus optical potential is derived from the Bonn nucleon-nucleon potential and the Dirac-Brueckner approach for nuclear matter. Our calculations, which do not contain any adjustable parameters, yield good agreement with experiment.

PACS number(s): 24.10.Jv, 25.40.Cm, 21.30.+y

I. INTRODUCTION

The microscopic description of the bulk properties of nuclear matter, finite nuclei, and nuclear reactions in terms of a realistic nucleon-nucleon (NN) interaction continues to be an interesting topic in nuclear physics. There are two aspects to the problem. First, one needs a realistic NN potential. This strong interaction should, in principle, be derived from quantum chromodynamics (QCD). However, up until now, attempts to derive the NN interaction from QCD have led only to very crude agreement with experiment which is unsuitable for studies of nuclear many-body systems. Presently, the only quantitative models for the nuclear force are based on meson exchange. Well-known examples for such realistic potentials are the Bonn [1,2] and the Paris [3] potentials; we will apply the former in this work.

The second aspect of the problem is a suitable many-body approach that is able to deal with a realistic NN interaction which has strong short-range components. The Brueckner approach and the variational method have been developed for this purpose. However, when using two-body forces in these nonrelativistic approaches, one is faced with a fundamental problem: Even the bulk properties of nuclear matter cannot be reproduced correctly [2,4].

Encouraged by the success of the Dirac phenomenology for nucleon-nucleus scattering [5,6] and the Walecka model for dense nuclear matter [7,8], a relativistic extension of the Brueckner method has been initiated by Shakin and co-workers [9,10], frequently called the Dirac-Brueckner-Hartree-Fock (DBHF) approach. This approach has been further developed by Brockmann and Machleidt [11,12] and by ter Haar and Malfliet [13]. Horowitz and Serot have discussed in detail the basic aspects involved in the derivation of the relativistic G matrix [14,15]. The common feature of all DBHF results is that a repulsive relativistic many-body effect is obtained which is strongly density dependent such that the empirical nuclear matter properties can be explained, starting from a realistic NN interaction.

There are basically two motivations for the extension of the DBHF approach to other observables of nuclear physics, e.g., nucleon-nucleus scattering. The first motivation is fundamental: One wants to test if it is possible to describe nuclear matter, finite nuclei, and nuclear reactions in terms of the same basic NN interaction. Second, the relativistic description of intermediate-energy nucleon-nucleus scattering is by itself an interesting topic of theoretical nuclear physics. Its most characteristic feature is the appearance of a strong attractive scalar and a strong repulsive vector potential, in terms of which the single-particle motion of the projectile nucleon in the mean field of the target nucleus can be described using the Dirac equation. In the Dirac phenomenology developed by Clark and collaborators [6,16,17], these potentials are adjusted to the nucleon-nucleus scattering data, using an appropriate number of parameters. Besides the Dirac phenomenology, approaches have been developed in which nucleon-nucleus scattering is described more microscopically. We mention here the relativistic impulse approximation [18–20] and calculations based on the Walecka model [21–23].

These approaches have some disadvantages. The Walecka model has no connection to the free-space NN interaction. In the relativistic impulse approximation, the medium effects are ingored. Thus it is tempting to develop a method that avoids both of these drawbacks. The DBHF calculation based on a realistic NN interactions offers this opportunity. There has been some work in this direction; e.g., in Refs. [13,24] the DBHF equations are solved directly in nuclear matter for a nucleon above the Fermi level.

In this paper we present an alternative approach which

combines the microscopic origin of the DBHF calculation with the simplicity of the Walecka model, such that an investigation of intermediate-energy nucleon-nucleus scattering is feasible.

The direct extension of the DBHF calculation from nuclear matter to finite nuclei and nuclear reactions is not trivial. More practically, one can parametrize the DBHF results for nuclear matter in terms of an effective Lagrangian which leads to the same predictions for nuclear matter as the original DBHF calculation. The effective Lagrangian, with its parameters derived from the realistic NN interaction, can then be used to investigate the properties of finite nuclei and nuclear reactions. Different schemes for this parametrization have been proposed [25–28]. We use in the present work a scheme similar to the one which was recently suggested by Brockmann and Toki [28]: The DBHF results for nuclear matter obtained from the Bonn potential are parametrized in terms of an effective σ-ω Lagrangian allowing for density-dependent meson-nucleon coupling constants.

We discuss in Sec. II the details of our calculation. The results and a discussion are presented in Sec. III. Finally a short summary is given in Sec. IV.

II. DETAILS OF THE CALCULATION

The one-boson-exchange (OBE) Bonn potential [2,29] used in this work is constructed in terms of the Thompson [30] equation. The kernel of this integral equation is the sum of one-meson-exchange amplitudes of six nonstrange bosons with given mass and coupling. Pseudovector (derivative) coupling is used for pseudoscalar mesons (π and η). A form factor of monopole type is applied to each meson-nucleon vertex which simulates the short-range dynamics of quark-gluon nature. See Refs. [2,29] for details about the OBE Bonn potential and its description of the two-nucleon system.

As in conventional Brueckner theory, the basic quantity in the DBHF approach is a reaction matrix $\tilde{G}$, which satisfies the in-medium Thompson equation. The nuclear matter properties are then obtained from this effective in-medium two-body interaction. Using the Bonn A potential [2], the DBHF calculation predicts that nuclear matter saturates at a density ρ=0.185 fm^{-3} and an energy per nucleon of −15.6 MeV, which is in good agreement with empirical information. More results and discussion concerning the properties of nuclear matter as obtained in the DBHF approach with the Bonn potential have been presented in Refs. [2,12,31]. In this work, we use the Bonn A potential [32].

As proposed by Brockmann and Toki [28], the DBHF results for nuclear matter can be parametrized by an effective Lagrangian, in analogy to the σ-ω model of Walecka:

$$\mathcal{L} = \overline{\psi}[i\gamma_\mu\partial^\mu - m - g_\sigma(\rho)\phi_\sigma - g_\omega(\rho)\gamma_\mu\phi_\omega^\mu]\psi + \tfrac{1}{2}(\partial^\mu\phi_\sigma)^2 - \tfrac{1}{2}m_\sigma^2\phi_\sigma^2 - \tfrac{1}{4}(\partial_\mu\phi_\omega^\nu - \partial_\nu\phi_\omega^\mu)^2 + \tfrac{1}{2}m_\omega^2\phi_\omega^{\mu 2}, \quad (1)$$

where ψ is the nucleon field, while ϕ_σ and ϕ_ω^μ are effective sigma and omega fields, respectively. The masses of the sigma and omega mesons, m_σ and m_ω, respectively, are kept fixed at their values in free-space scattering (m_σ = 550 MeV, m_ω = 782.6 MeV). However, the coupling constants of these effective mesons, g_σ and g_ω, depend on the baryon density ρ. They are determined from the DBHF results for nuclear matter.

The (complex) nucleon self-energy produced by the effective meson exchanges in nuclear matter can, in general, be written as

$$\Sigma(k_\mu) = \Sigma_S(k_\mu) + \gamma^0\Sigma_0(k_\mu) + \gamma\cdot\mathbf{k}\Sigma_V(k_\mu) = V + iW, \quad (2)$$

where Σ_S, Σ_0, and Σ_V denote the scalar component, the timelike part of the vector component, and the spacelike part of the vector component of the nucleon self-energy, respectively.

In our notation, k_μ stands for all four components of the momentum four-vector, and $k \equiv |\mathbf{k}|$.

Treating the effective coupling constants locally as numbers and calculating in the relativistic Hartree-Fock approximation [see Figs. 1(a) and 1(b) for the corresponding Feynman diagrams], we obtain the explicit expressions for the real part of the nucleon self-energy [8,21,23],

$$V_S(k,\rho) = -\left(\frac{g_\sigma(\rho)}{m_\sigma}\right)^2\rho_S + \frac{1}{16\pi^2 k}\int_0^{k_F} dqq\frac{m_q^*(\rho)}{E_q^*(\rho)}\{g_\sigma^2(\rho)\Theta_\sigma(k,q) - 4g_\omega^2(\rho)\Theta_\omega(k,q)\}, \quad (3)$$

$$V_0(k,\rho) = \left(\frac{g_\omega(\rho)}{m_\omega}\right)^2\rho + \frac{1}{16\pi^2 k}\int_0^{k_F} dqq\{g_\sigma^2(\rho)\Theta_\sigma(k,q) + 2g_\omega^2(\rho)\Theta_\omega(k,q)\}, \quad (4)$$

$$V_V(k,\rho) = -\frac{1}{8\pi^2 k^2}\int_0^{k_F} dqq\frac{q^*}{E_q^*(\rho)}\{g_\sigma^2(\rho)\Phi_\sigma(k,q) + 2g_\omega^2(\rho)\Phi_\omega(k,q)\}, \quad (5)$$

where

$$\rho_S = 4\int_0^{k_F}\frac{d^3q}{(2\pi)^3}\frac{m_q^*(\rho)}{E_q^*(\rho)},$$

$$\rho = 4\int_0^{k_F}\frac{d^3q}{(2\pi)^3},$$

and

$$\Theta_i(k,q) = \ln\left|\frac{(k+q)^2 + m_i^2 - (q_0 - k_0)^2}{(k-q)^2 + m_i^2 - (q_0 - k_0)^2}\right|,$$

$$\Phi(k,q) = \frac{k^2 + q^2 + m_i^2 - (k_0 - q_0)^2}{4kq}\Theta_i(k,q) - 1,$$

$$i = \sigma, \omega.$$

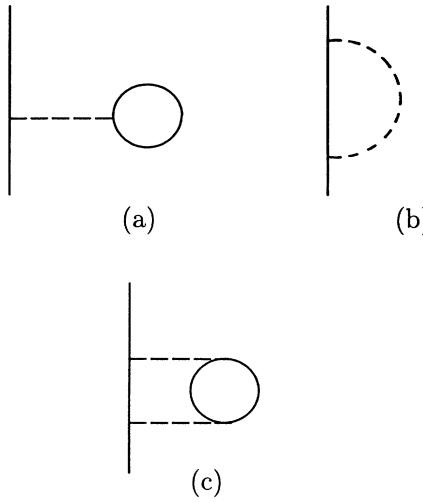

FIG. 1. Feynman diagrams for the calculation of the nucleon self-energy in nuclear matter. (a) Hartree contribution, (b) Fock contribution, (c) fourth-order contribution.

The effective mass m^*, the kinetic momentum $\mathbf{k}^*$, and the single-particle energy k_0 are given by

$$m_k^*(\rho) = m + V_S(k,\rho),$$
$$\mathbf{k}^* = \mathbf{k}[1 + V_V(k)],$$
$$k_0 = E_k^* + V_0 = (\mathbf{k}^{*2} + m_k^{*2})^{1/2} + V_0,$$

and similarly for q.

The first term of V_S and V_0 is the momentum-independent Hartree contribution [see Fig. 1(a)], while the other terms are the Fock contributions [see Fig. 1(b)] which depend on k. A very small spacelike component of the vector potential is due entirely to Fock diagrams.

In order to determine the effective coupling constants from these expressions, we drop the spacelike component of the vector potential [Eq. (5)] and calculate V_S [Eq. (3)] and V_0 [Eq. (4)] for $k = k_F$, which are then identified with the scalar and vector potentials obtained in the DBHF calculation (see Table VII of Ref. [12]). This is a reasonable assumption since the spacelike component of the vector potential is very small and the potentials are only very weakly momentum dependent [33]. Note that these approximations are used only for the determination of the effective coupling constants; in the calculation of the optical potential, the spacelike part of the vector potential [Eq. (5)] is taken into account [see Eq. (10) below]. The momentum k in Eqs. (3)–(5) is related to the incident energy of the projectile [see Eq. (11) below] through $k_0 = E$. Both effective coupling constants drop with increasing density [34,35].

The lowest-order contribution to the imaginary part of the nucleon self-energy is obtained from the fourth-order (counting the meson-nucleon vertices) Feynman diagrams which are characterized by two-particle–one-hole (2p1h) intermediate states [see Fig. 1(c)]. The nucleon lines in these Feynman diagrams are described by dressed nucleon propagators, which corresponds to performing the calculation on the Hartree-Fock ground state. The imaginary part of nucleon self-energy due to the fourth-order Feynman diagrams can be expressed as [22,23]

$$W_S(k,\rho) = \frac{1}{8\pi^2 k}\int_0^{E'} dq_0 \int_{|k-p|}^{k+p} dqq\Big[g_\sigma^2(\rho)m^*\Delta_\sigma^2(q)\mathrm{Im}\pi_\sigma(q) + g_\omega^2(\rho)m^*\Delta_\omega^2(q)g_{\mu\lambda}\mathrm{Im}\pi_\omega^{\lambda\mu}(q) + 2g_\sigma(\rho)g_\omega(\rho)(E_\mathbf{k}^* - \frac{1}{2}q_0)\frac{q_\mu^2}{q^2}\Delta_\sigma(q)\Delta_\omega(q)\mathrm{Im}\pi_{\sigma\omega}^0(q)\Big], \tag{6}$$

$$W_0(k,\rho) = \frac{1}{8\pi^2 k}\int_0^{E'} dq_0 \int_{|k-p|}^{k+p} dqq\Big\{g_\sigma^2(\rho)\Delta_\sigma^2(q)(E_\mathbf{k}^* - q_0)\mathrm{Im}\pi_\sigma(q) - g_\omega^2(\rho)\Delta_\omega^2(q)\Big[(E_\mathbf{k}^* - q_0)g_{\mu\lambda}\mathrm{Im}\pi_\omega^{\lambda\mu}(q) + (2E_\mathbf{k}^* - q_0)\frac{q_\mu^2}{q^2}\mathrm{Im}\pi_\omega^{00}(q)\Big] - 2g_\sigma(\rho)g_\omega(\rho)m^*\Delta_\sigma(q)\Delta_\omega(q)\mathrm{Im}\pi_{\sigma\omega}^0(q)\Big\}, \tag{7}$$

$$W_V(k,\rho) = -\frac{1}{8\pi^2 k^3}\int_0^{E'} dq_0 \int_{|k-p|}^{k+p} dqq\Big\{g_\sigma^2(\rho)\Delta_\sigma^2(q)[k^2 + \tfrac{1}{2}q_\mu^2 - E_\mathbf{k}^* q_0)]\mathrm{Im}\pi_\sigma(q) + g_\omega^2(\rho)\Delta_\omega^2(q)\Big[-(k^2 + \tfrac{1}{2}q_\mu^2 - E_\mathbf{k}^* q_0)g_{\mu\lambda}\mathrm{Im}\pi_\omega^{\lambda\mu}(q) + \frac{q_0 q_\mu^2}{q^4}(2E_\mathbf{k}^* q_0 - q_\mu^2)(\tfrac{1}{2}q_0 - E_\mathbf{k}^*)\mathrm{Im}\pi_\omega^{00}(q)\Big] - g_\sigma(\rho)g_\omega(\rho)m^*\frac{q_0}{q}(2k_0^* q_0 - q_\mu^2)\Delta_\sigma(q)\Delta_\omega(q)\mathrm{Im}\pi_{\sigma\omega}^0(q)\Big\}, \tag{8}$$

where q is the magnitude of the three-vector q, while

$$m^* = m_k^*(\rho),$$

$$E' = E_{\mathbf{k}}^* - (k_F^2 + m^{*2})^{1/2},$$

$$p = [(E_{\mathbf{k}}^* - q_0)^2 - m^{*2}]^{1/2},$$

$$q_\mu^2 = q_\mu q^\mu,$$

$$\Delta_i(q) = \frac{1}{q_\mu^2 - m_i^2}, \quad i = \sigma,\ \omega,$$

and $\pi(q)$ are meson polarization insertions; their imaginary parts are

$$\mathrm{Im}\pi_\sigma(q) = -\frac{g_\sigma^2(\rho)}{\pi q}(m^{*2} - \tfrac{1}{4}q_\mu^2)(E_F^* - E^*),$$

$$\mathrm{Im}g_{\mu\lambda}\pi_\omega^{\lambda\mu}(q) = -\frac{g_\omega^2(\rho)}{\pi q}(m^{*2} + \tfrac{1}{2}q_\mu^2)(E_F^* - E^*),$$

$$\mathrm{Im}\pi_\omega^{00}(q) = -\frac{g_\omega^2(\rho)}{\pi q}[\tfrac{1}{3}(E_F^{*3} - E^{*3}) + \tfrac{1}{2}(E_F^{*2} - E^{*2})q_0 + \tfrac{1}{4}q_\mu^2(E_F^* - E^*)],$$

$$\mathrm{Im}\pi_{\sigma\omega}^0(q) = -\frac{g_\sigma(\rho)g_\omega(\rho)}{2\pi q}m^*[(E_F^{*2} - E^{*2}) + (E_F^* - E^*)q_0],$$

where

$$E^* = \max\{E_r, E_F^* - q_0, m^*\},$$

$$E_r = -\tfrac{1}{2}q_0 + \tfrac{1}{2}q(1 - 4m^*/q_\mu^2)^{1/2},$$

$$E_F^* = (k_F^2 + m^{*2})^{1/2}.$$

The derivation of the nucleon self-energy [Eqs. (3)–(8)] from the Walecka model has been discussed in detail in Refs. [21,22]. For the effective Lagrangian [Eq. (1)] used in the present work, the expressions for the nucleon self-energy are the same, only with the coupling constants of the sigma and omega exchanges replaced by those determined from the DBHF approach which are now density dependent.

The same fourth-order diagrams which yield the imaginary part also give rise to a contribution to the real part of the self-energy, which should be added to the Hartree-Fock term. Note, however, that the Hartree-Fock contribution has been derived from a G-matrix description of nuclear matter and therefore already contains these terms in a certain approximation. In order to avoid any double counting no contributions of the fourth-order diagram to the real part have been considered.

The nucleon self-energy in a finite nucleus is obtained by means of the local density approximation, in which the spatial dependence of the microscopic optical potential is directly related to the density of the target nucleus. For a self-consistent description of nucleon-nucleus scattering (by self-consistency we mean that there are no free parameters after the NN potential has been selected), the target density should also be determined from the effective Lagrangian, Eq. (1). In this paper, we use the density determined in the relativistic density-dependent Hartree-Fock (RDHF) calculation with the effective Lagrangian of Eq. (1) [35]. For comparison, we also use the density determined in a relativistic density-dependent Hartree (RDH) calculation [35], as well as the density determined in the relativistic Hartree (RH) calculation with the Walecka model [36]. As shown in Ref. [35], the RDH results for the binding energy and root-mean-square radius of ^{40}Ca are in good agreement with experiment, while the RDHF results slightly underestimates them.

The Dirac equation for the single-particle motion of the projectile nucleon in the mean field of the target nucleus can be written as

$$[\alpha\cdot\mathbf{k} + \beta(m + U_S) + U_V + V_C]\psi = E\psi, \tag{9}$$

with

$$U_S = \frac{\Sigma_S - m\Sigma_V}{1 + \Sigma_V}, \quad U_V = \frac{\Sigma_0 + E\Sigma_V}{1 + \Sigma_V}, \tag{10}$$

where E is the energy of the projectile in the center-of-mass (c.m.) system of projectile and nucleus, which is related to the incident energy T_{lab} through

$$E = E_{p,\mathrm{c.m.}} = \frac{m^2 + m_T(m + T_{\mathrm{lab}})}{[(m + m_T)^2 + 2m_T T_{\mathrm{lab}}]^{1/2}}, \tag{11}$$

with m and m_T the mass of the projectile and target, respectively. V_C is the Coulomb field which we treat in the same way as in Refs. [20,36].

In order to calculate the experimental observables, the Dirac equation is usually converted into a Schrödinger-equivalent equation. The Dirac equation for the four-component spinor ψ is equivalent to two coupled equations for the large (upper) and small (lower) two-component spinors. One can eliminate the small component of the Dirac spinor in a standard way and obtain a Schrödinger-equivalent equation for the large component of the Dirac spinor [6,20,36],

$$\left[\frac{\mathbf{k}^2}{2E} + U_{\mathrm{eff}}(r) + V_C(r) + U_{\mathrm{s.o.}}(r)\sigma\cdot\mathbf{l}\right]\phi(\mathbf{r}) = \frac{E^2 - m^2}{2E}\phi(\mathbf{r}), \tag{12}$$

where U_{eff} and $U_{\mathrm{s.o.}}$ are the central and the spin-orbit parts of the Schrödinger-equivalent potential, which is known as the nucleon-nucleus optical potential in non-relativistic approaches. The explicit expressions for U_{eff} and $U_{\mathrm{s.o.}}$ are

$$U_{\mathrm{eff}} = U_V + \frac{1}{2E}[U_S(2m + U_S) - (U_V + V_C)^2 + U_{\mathrm{Darwin}}], \tag{13}$$

$$U_{\text{s.o.}} = -\frac{1}{2ErD(r)}\frac{dD(r)}{dr}, \tag{14}$$

with

$$U_{\text{Darwin}} = \frac{3}{4}\left[\frac{1}{D(r)}\frac{dD(r)}{dr}\right]^2 - \frac{1}{rD(r)}\frac{dD(r)}{dr} - \frac{1}{2D(r)}\frac{d^2D(r)}{dr^2},$$

$$D(r) = m + E + U_S - U_V - V_C.$$

III. RESULTS AND DISCUSSION

We show in Fig. 2 the density of ^{40}Ca determined in a RDHF (solid curve) and RDH (dashed curve) calculation [35] using the effective Lagrangian of Eq. (1); they are compared with the density (dotted curve) as obtained from a relativistic Hartree (RH) calculation applying the Walecka model (QHD-I) [36]. Note that the RDHF calculation slightly underestimates the root-mean-square radius of ^{40}Ca [35].

We show in Fig. 3 the scalar potential U_S and vector potential U_V for p+^{40}Ca scattering obtained in the present calculation. The RDHF density is used in the local density approximation. The real parts of these potentials are only weakly energy dependent; in the interior of the nuclei, they are about −420 and +320 MeV, respectively. The overwhelming part of these real potentials comes from the energy-independent Hartree contribution; the energy-dependent Fock contribution plays only a minor role. On the other hand the imaginary part of the scalar and vector potentials depends of course very strongly on the energy; both increase in magnitude with increasing energy. Note that the radial shapes of the real Dirac potentials follow essentially that of the target density (cf. solid curve in Fig. 2).

With the nucleon self-energy determined from the effective Lagrangian which is related to the realistic NN interaction used in the DBHF calculation, we can obtain the Schrödinger-equivalent potential through Eqs. (13) and (14) which is then used in Eq. (12) to calculate the experimental observables [36]. The Schrödinger-equivalent potentials, corresponding to the Dirac potentials in Fig. 3, are shown in Fig. 4. As can be seen from the figure, the real part of the central potential is strongly energy dependent. At low incident energy (T_{lab}=150) the real part of the central potential is attractive throughout the whole radial space and has a longer range. With the increase of the incident energy, the real part of the central potential becomes less attractive and is repulsive in the interior of the nucleus when T_{lab}=300 MeV. A typical pocket of attraction is observed at the nuclear surface at this energy. At even higher energy (T_{lab}=450 MeV), the real central potential is repulsive in the whole radial space. The imaginary part of the central potential also shows a strong energy dependence. The imaginary central potential is negative at all energies; its magnitude increases while its range decreases with increasing energy.

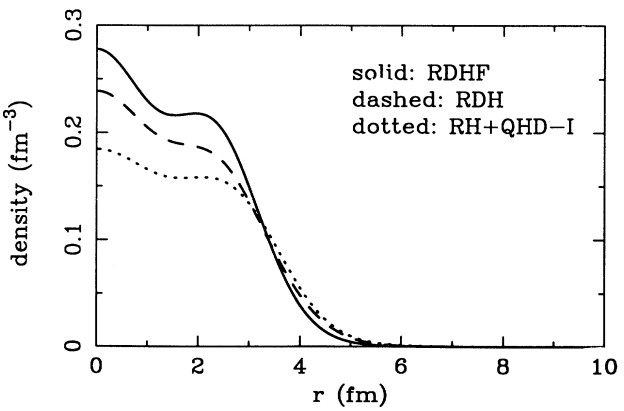

FIG. 2. Nucleon density of ^{40}Ca as obtained in RDHF (solid curve) and RDH (dashed curve) calculations with the effective Lagrangian, Eq. (1) [35]; the dotted curve represents a RH calculation with the Walecka (QHD-I) model [36].

The important feature of the relativistic approach is that the spin-orbit potential arises naturally from the coherent sum of the contributions from the scalar and vector potentials. While the real part of the spin-orbit potential is attractive, its imaginary part is mostly positive. The real part of the spin-orbit potential decreases (in magnitude) with increasing incident energy, whereas its imaginary part increases with the energy. The fluctuations of the spin-orbit potential in the interior of the nucleus are due to fluctuations in the target density (cf. solid curve in Fig. 2).

The results for differential cross sections and analyzing powers in elastic p+^{40}Ca scattering at T_{lab}=300 and 400 MeV are shown in Fig. 5 and Fig. 6, respectively. In these figures, the solid and dashed curves are the results of our calculations with RDHF and RDH densities, respectively, while for the dotted curves the RH density from the Walecka model (QHD-I) [36] is used. The experimental data are from Ref. [37].

For full self-consistency of our calculations, we must use the RDHF density since it is based upon the same effective coupling constants as our optical potential. With the RDHF density, our results (solid curves) are in reasonable agreement with experiment. The agreement is particularly good at small angles ($\theta_{\text{c.m.}} \leq 15°$). At large angles, we overestimate the experimental differential cross section. The oscillations in the differential cross section and analyzing power seem to have a larger period than the experimental data show (note that there is a correspondence between the minima in the differential cross section and the dips in the analyzing power). Since our calculations are parameter free, the quality of agreement with the experimental data is remarkable. The remaining discrepancies are probably mainly due to the fact that the target density as obtained in the RDHF calculation underestimates the root-mean-square radius [35] (see discussion below).

When using the RDH density, which is in better agreement with the experimental root-mean-square radius [35], our results (dashed curves in Figs. 5 and 6) improve; and there is further improvement when the RH density (dotted curves) is used. Thus, the accurate reproduction

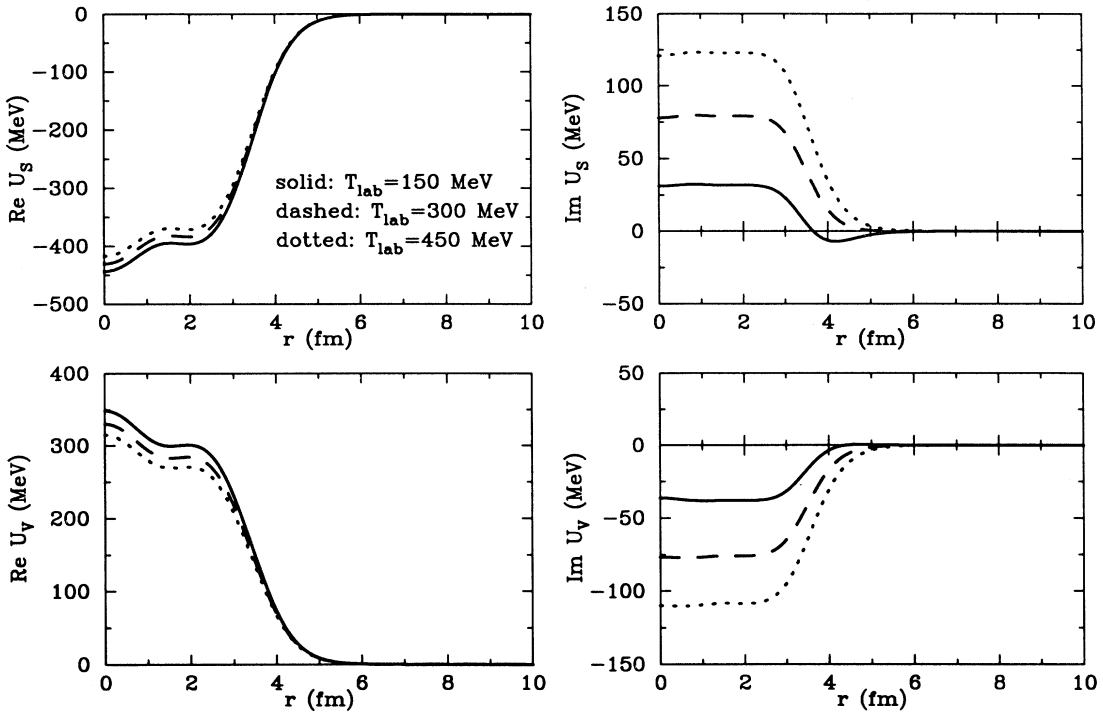

FIG. 3. Scalar and vector potentials in p+^{40}Ca scattering at 150 (solid curves), 300 (dashed curves), and 450 MeV (dotted curves). The RDHF density is used in local density approximation.

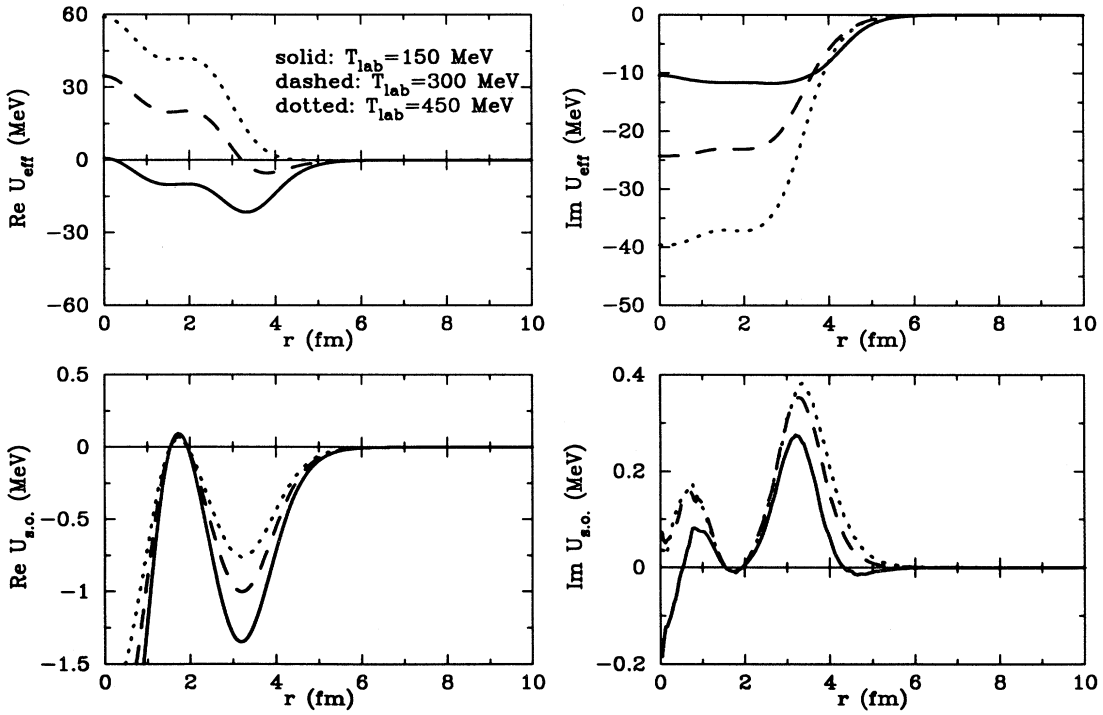

FIG. 4. The Schrödinger-equivalent potential in p+^{40}Ca scattering at 150 (solid curves), 300 (dashed curves), and 450 MeV (dotted curves). The RDHF density is used in local density approximation.

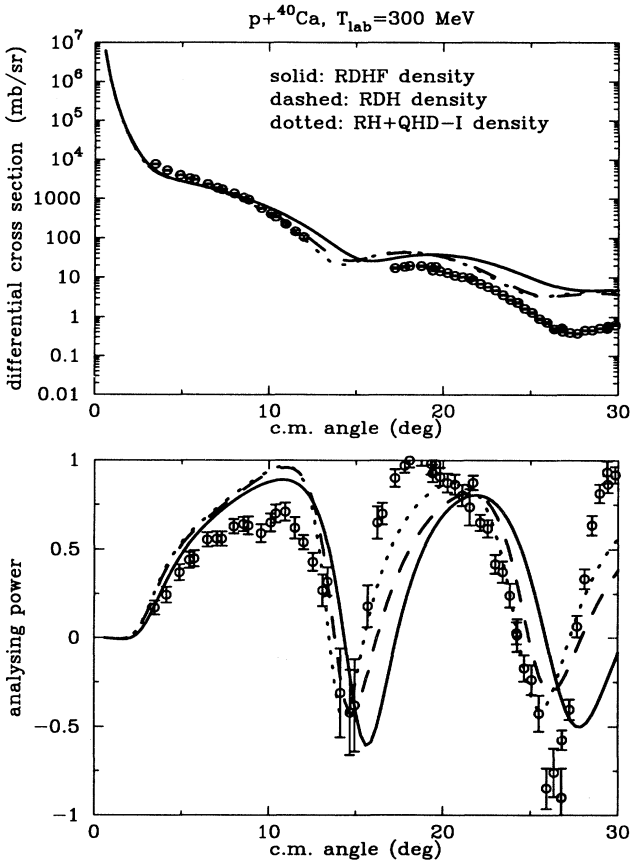

FIG. 5. Elastic differential cross section and analyzing power in p+^{40}Ca scattering at $T_{\rm lab}$=300 MeV. The solid and dashed curves are the predictions by the present calculations with RDHF (solid curve in Fig. 2) and RDH (dashed curve in Fig. 2) densities, respectively, while the dotted curves are the results using the RH density from the Walecka (QHD-I) model (dotted curve in Fig. 2). The experimental data are from Ref. [37].

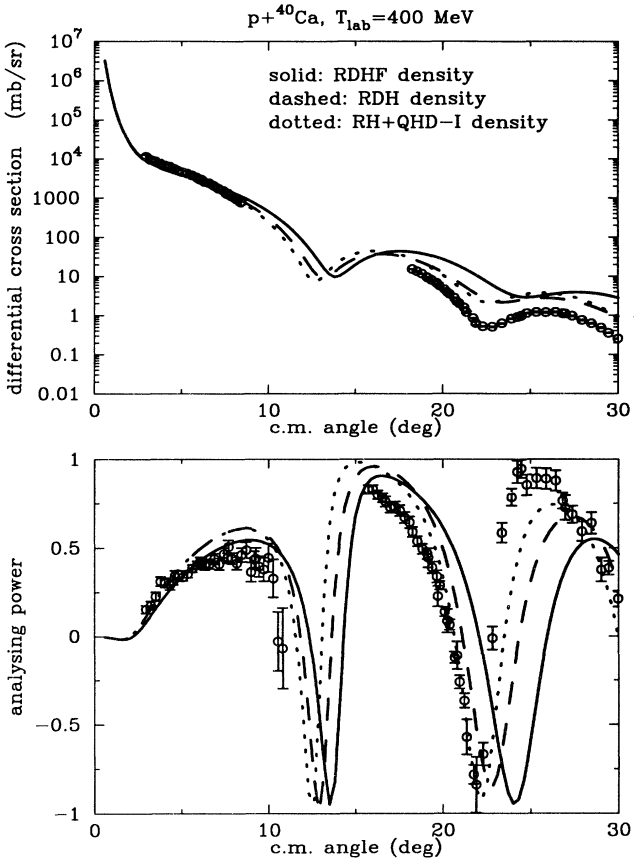

FIG. 6. Same as Fig. 3, but at $T_{\rm lab}$=400 MeV.

of the nucleon density of finite nuclei is probably the most important outstanding problem for the self-consistent description of nuclear structure and nuclear reactions.

IV. SUMMARY

In this paper, we have continued our efforts of obtaining a parameter-free and self-consistent description of nuclear matter, finite nuclei, and nuclear reactions in terms of one realistic NN interaction. Here, we have studied p+^{40}Ca scattering in Dirac dynamics. In order to carry out a systematic study, we parametrized the DBHF results for nuclear matter in terms of a simple effective Lagrangian consisting of an attractive sigma exchange and a repulsive omega exchange. The coupling constants of these effective mesons are density dependent and are determined from the DBHF results for nuclear matter.

The nucleon self-energy in nuclear matter is then calculated based on the effective Lagrangian up to the fourth-order Feynman diagrams. The nucleon-nucleus optical potential in finite nuclei is related to the self-energy in nuclear matter by means of the local density approximation, where the target density is determined by the same effective Lagrangian as the nucleon self-energy. Furthermore, the Dirac equation describing the single-particle motion of the projectile in the mean field of the target is converted to the Schrödinger-equivalent equation which is solved to obtain the observables.

With the optical potential thus determined, we have calculated observables of p+^{40}Ca scattering at intermediate energies. The predictions by our model for the elastic differential cross section and the analyzing power were compared with the experimental data. The agreement between our parameter-free calculations and experiment is remarkable. At large scattering angles, our results for the differential cross section overestimate the experimental data. This can be attributed, in part, to small deficiencies in the densities as obtained in the RDHF calculation.

ACKNOWLEDGMENTS

One of the authors (G.Q.L.) would like to thank Professor W. C. Olsen for the experimental data file. This work was supported in part by the U.S. National Science Foundation under Grant No. PHY-9211607 and by the Idaho State Board of Education.

[1] R. Machleidt, K. Holinde, and Ch. Elster, Phys. Rep. **149**, 1 (1987).
[2] R. Machleidt, Adv. Nucl. Phys. **19**, 189 (1989).
[3] M. Lacombe, B. Loiseau, J. M. Richard, R. Vinh Mau, J. Cote, P. Pires, and R. de Tourreil, Phys. Rev. C **21**, 861 (1980).
[4] B. D. Day and R. B. Wiringa, Phys. Rev. C **32**, 1057 (1985).
[5] L. G. Arnold, B. C. Clark, and R. L. Mercer, Phys. Rev. C. **19**, 917 (1979).
[6] B. C. Clark, in *Relativistic Dynamics and Quark-Nuclear Structure*, edited by M. B. Johnson and A. Picklesimer (Wiley, New York, 1986).
[7] J. D. Walecka, Ann. Phys. (N.Y.) **83**, 491 (1974).
[8] B. D. Serot and J. D. Walecka, Adv. Nucl. Phys. **16**, 1 (1986).
[9] M. R. Ansatasio, L. S. Celenza, W. S. Pong, and C. M. Shakin, Phys. Rep. **100**, 327 (1983).
[10] L. S. Celenza and C. M. Shakin, *Relativistic Nuclear Physics: Theories of Structure and Scattering,* Lecture Notes in Physics Vol. 2 (World Scientific, Singapore, 1986).
[11] R. Brockmann and R. Machleidt, Phys. Lett. **149B**, 283 (1984).
[12] R. Brockmann and R. Machleidt, Phys. Rev. C **42**, 1965 (1990).
[13] B. ter Haar and R. Malfliet, Phys. Rep. **149**, 207 (1987).
[14] C. J. Horowitz and B. D. Serot, Phys. Lett. **137B**, 287 (1984).
[15] C. J. Horowitz and B. D. Serot, Nucl. Phys. **A464**, 613 (1987).
[16] S. Hama, B. C. Clark, E. D. Cooper, H. S. Sherif, and R. L. Mercer, Phys. Rev. C **41**, 2737 (1990).
[17] E. D. Cooper, S. Hama, B. C. Clark, and R. L. Mercer, Phys. Rev. C **47**, 297 (1993).
[18] J. A. McNeil, J. R. Shepard, and S. J. Wallace, Phys. Rev. Lett. **50**, 1493 (1983).
[19] S. J. Wallace, Annu. Rev. Nucl. Part. Sci. **37**, 267 (1987).
[20] D. P. Murdock and C. J. Horowitz, Phys. Rev. C **35**, 1442 (1987).
[21] C. J. Horowitz and B. D. Serot, Nucl. Phys. **A399**, 529 (1983).
[22] C. J. Horowitz, Nucl. Phys. **A412**, 228 (1984).
[23] Z. Y. Ma, P. Zhu, Y. Q. Gu, and Y. Z. Zhuo, Nucl. Phys. **A490**, 619 (1988).
[24] Y. Miyama, Phys. Lett. B **215**, 602 (1988).
[25] H. Elsenhans, H. Müther, and R. Machleidt, Nucl. Phys. **A515**, 715 (1990).
[26] S. Marcos, M. Lopez-Quelle, and N. Van Giai, Phys. Lett. B **257**, 5 (1991).
[27] S. Gmuca, Nucl. Phys. **A547**, 447 (1992).
[28] R. Brockmann and H. Toki, Phys. Rev. Lett. **68**, 340 (1992).
[29] R. Machleidt, in *Computational Nuclear Physics*, edited by S. E. Koonin, K. Langanke, and A. Maruhn (Springer, New York, 1993), Vol. II, p. 1.
[30] R. H. Thompson, Phys. Rev. D **1**, 710 (1970).
[31] G. Q. Li, R. Machleidt, and R. Brockmann, Phys. Rev. C **45**, 2782 (1992).
[32] The Bonn *A* potential, which is applied in the present work, is defined in Table A.2 of Ref. [2].
[33] R. Machleidt, in *Relativistic Dynamics and Quark-Nuclear Physics*, edited by M. B. Johnson and A. Picklesimer (Wiley, New York, 1986), p. 71.
[34] G. Q. Li, R. Machleidt, and Y. Z. Zhuo, Phys. Rev. C (submitted).
[35] R. Fritz, H. Müther, and R. Machleidt, Phys. Rev. Lett. **71**, 46 (1993).
[36] C. J. Horowitz, D. P. Murdock, and B. D. Serot, in *Computational Nuclear Physics*, edited by K. Langanke, A. Maruhn, and S. E. Koonin (Springer, New York, 1991), Vol. I.
[37] D. A. Hutcheon *et al.*, Nucl. Phys. **A483**, 429 (1988); W. C. Olsen (private communication).